

RESEARCH ARTICLE

View Article Online
View Journal | View IssueCite this: *Inorg. Chem. Front.*, 2022, **9**, 5805

Carbon cage isomers and magnetic Dy...Dy interactions in Dy₂O@C₈₈ and Dy₂C₂@C₈₈ metallofullerenes†

Wei Yang,^{‡a,b} Georgios Velkos,^{‡a} Svetlana Sudarkova,^a Bernd Büchner,^a Stanislav M. Avdoshenko,^{*a} Fupin Liu,^{†a} Alexey A. Popov,^{†a} and Ning Chen,^{†b}

Three isomers of Dy₂O@C₈₈ and two isomers of Dy₂C₂@C₈₈ were synthesized and structurally characterized by single-crystal X-ray diffraction, vibrational spectroscopy, and DFT calculations. Both types of clusterfullerenes feature 4-fold electron transfer to the carbon cage, thus resulting in the same carbon cage isomers identified as C₁(26), C₅(32), and D₂(35). The studies of Dy...Dy superexchange interactions in Dy₂O and Dy₂C₂ clusters revealed that the O²⁻ bridge favors antiferromagnetic coupling whereas the acetylide group C₂²⁻ supports ferromagnetic coupling of Dy magnetic moments. The strength of the coupling showed a considerable variability in different cage isomers. All metallofullerenes exhibited slow relaxation of magnetization and magnetic hysteresis. In Dy₂O@C₈₈ isomers the hysteresis remained open up to 7–9 K, while in Dy₂C₂@C₈₈ the hysteresis loops were closed already at 2.5 K. This study demonstrated that both the endohedral bridge between metal atoms and the fullerene cage play an important role in magnetic interactions and relaxation of magnetization.

Received 17th August 2022,
Accepted 25th September 2022
DOI: 10.1039/d2qi01796b

rsc.li/frontiers-inorganic

Introduction

Endohedral metallofullerenes (EMFs) feature fascinating structural diversity, defined by a broad variability of endohedral species with 1–4 metal ions, which are encapsulated in carbon cages of various shape and size ranging from C₆₆ to C₁₀₈ and beyond.^{1–5} In clusterfullerenes, endohedral species also include some non-metal atoms, which acquire a negative charge and serve as bridges between metals.^{6,7} The non-metal then defines the names of clusterfullerenes, such as endohedral oxygen in oxide clusterfullerenes^{8,9} or endohedral carbon in carbide clusterfullerenes.^{10,11}

The exploration of oxide clusterfullerenes started with a discovery of Sc₄O_{2,3}@C₈₀ by Stevenson *et al.*^{12,13} and then continued with a series of Sc₂O@C_{2n} EMFs with cage sizes from C₇₀ to C₈₂.^{14–20} More recently, the focus was shifted to lanthanides, resulting in several M₂O@C_{2n} EMFs with Ho (C_{2n} = C₇₄,²¹

C₈₄,²² 4 isomers of C₉₀,²³ and 2 isomers of C₉₂²⁴), Dy (C_{2n} = C₇₂,²⁵ C₇₄,²⁵ C₈₀,²⁶ three isomers of C₈₂²⁷), and two isomers of Lu₂O@C₈₀.²⁸ In M₂O@C_{2n} clusterfullerenes, two rare-earth metal ions (M³⁺) are bridged by the μ₂-O²⁻ ion; the whole M₂O cluster has a formal charge of +4 and is encapsulated in fullerene cages preferring the C_{2n}⁴⁻ state.

A special interest in Dy-EMFs is motivated by their magnetic properties.²⁹ In lanthanide clusterfullerenes, the non-metal ions bear a large negative charge, which imposes a strong axial ligand field and large magnetic anisotropy of nearby lanthanide ions. At the same time, isolation of endohedral species inside the carbon cage enables rather uncommon and yet simple atomic arrangements, thus creating a platform for the study of magnetic interactions and relaxation phenomena, especially well established for Dy-EMFs. But the carbon cage is not just an inert container for encapsulated clusters. A size and shape of a fullerene and topology of its π-system not only determine the electronic properties of the host but also affect the properties of the guests. An intriguingly strong variation of the magnetic properties found for Dy₂O@C_{2n} clusterfullerenes with C₇₂–C₈₂ cages^{25–27} calls for a systematic study of this factor, and in this work we focus on the larger fullerene cage, C₈₈, for which we isolate three isomers of Dy₂O@C₈₈, determine their molecular structures and analyze magnetic properties.

While oxide clusterfullerenes based on C₈₈ were not reported yet, this cage is known for other EMFs with 4-fold

^aLeibniz Institute for Solid State and Materials Research (IFW Dresden), Helmholtzstrasse 20, 01069 Dresden, Germany. E-mail: f.liu@ifw-dresden.de, s.avdoshenko@ifw-dresden.de, a.popov@ifw-dresden.de

^bCollege of Chemistry, Chemical Engineering and Materials Science, Soochow University, Suzhou, Jiangsu 215123, P. R. China. E-mail: chenning@suda.edu.cn

†Electronic supplementary information (ESI) available. CCDC 2175825–2175828. For ESI and crystallographic data in CIF or other electronic format see DOI: <https://doi.org/10.1039/d2qi01796b>

‡These authors contributed equally.



electron transfer, such as dimetallofullerenes $\text{Sm}_2@C_{88}$ ³⁰ and $\text{Lu}_2@C_{88}$ ³¹ and carbide clusterfullerenes $\text{M}_2\text{C}_2@C_{88}$ ($\text{M} = \text{Sc}$,³² Y ,³³ Er ,³⁴ and Lu ;^{31,35} see Table 1). The structural studies revealed four cage isomers of C_{88} in those EMFs, including three classical fullerenes $C_1(26)$, $C_s(32)$, and $D_2(35)$, and one heptagon-containing isomer with C_s symmetry (labeled as $C_s(\text{hept})$). As both feature 4-fold electron transfer to the fullerene, it is reasonable to expect similarity of the cage structure of oxide and carbide clusterfullerenes, and we anticipated to find these cage isomers for $\text{Dy}_2\text{O}@C_{88}$ as well. But this structural similarity also allows a different question to be addressed – how the bridge between two Dy ions affects magnetic properties and in particular Dy...Dy coupling. This problem requires a study of different types of clusterfullerenes sharing the same fullerene cages, and therefore we also decided to synthesize $\text{Dy}_2\text{C}_2@C_{88}$ isomers for comparison with $\text{Dy}_2\text{O}@C_{88}$ counterparts. Furthermore, magnetic properties of Dy_2C_2 clusterfullerenes remain poorly explored, except for a single study of $\text{Dy}_2\text{C}_2@C_s(6)-C_{82}$, and thus analysis of the role of acetylide group in $\text{Dy}_2\text{C}_2@C_{2n}$ EMFs with different cages is an important task on its own.

Synthesis and separation

For the synthesis of Dy_2O -clusterfullerenes, core-drilled graphite rods filled with Dy_2O_3 /graphite powder mixture were evaporated in arc-discharge under He/CO_2 (270/27 mbar) atmosphere. The soot was collected and extracted by carbon disulfide (CS_2) under an argon atmosphere for 12 h. The crude extract, containing mainly empty fullerenes, Dy-monometallofullerenes, and Dy_2O -oxide clusterfullerenes, was treated with TiCl_4 following the method proposed by Shinohara *et al.*^{36,37} While empty fullerenes did not react with TiCl_4 , Dy-EMFs formed an insoluble complex and could be separated by filtration and then released by breaking the complex with water (Fig. S1†). Three isomers of $\text{Dy}_2\text{O}@C_{88}$ were then isolated from the recovered EMF mixture after several steps of linear and recycling HPLC (Fig. S2†) and characterized by LDI-TOF mass-spectrometry as described in ESI (Fig. S3†). The isomers are denoted as **Dy₂O-I**, **Dy₂O-II**, and **Dy₂O-III**, where the Roman number corresponds to the retention time of a given isomer during HPLC separation.

Dy_2C_2 -clusterfullerenes were synthesized by a similar arc-discharge process, but using He atmosphere with the addition

of N_2 (180/10 mbar). The CS_2 extract of the soot in this case contained mainly empty fullerenes, Dy-monometallofullerenes, Dy_3N -nitride clusterfullerenes, and Dy_2C_2 -carbide clusterfullerenes. Following the SAFA approach developed by Stevenson *et al.*,^{38–40} the extract was re-dissolved in toluene and reacted with dried diamino silica gel (DASG). Empty fullerenes, Dy-monometallofullerenes, and Dy_2C_2 -clusterfullerenes reacted with amino groups and were trapped by DASG, whereas less reactive $\text{Dy}_3\text{N}@C_{2n}$ clusterfullerenes mainly remained in solution. The DASG with immobilized fullerenes was then filtered and washed with CS_2 , which resulted in the release of $\text{Dy}_2\text{C}_2@C_{2n}$, whereas Dy-monometallofullerenes and main part of empty fullerenes remained trapped (Fig. S4†). Two isomers of $\text{Dy}_2\text{C}_2@C_{88}$ denoted as **Dy₂C₂-I** and **Dy₂C₂-II** (the Roman numbers correspond to the retention time), were then isolated by HPLC (Fig. S5†) and characterized by LDI-TOF mass-spectrometry as described in ESI† (Fig. S6).

Molecular structures

Single-crystal X-ray diffraction

Molecular structures of **Dy₂O-I**, **Dy₂C₂-I**, **Dy₂C₂-II**, and **Dy₂O-III** were established by single-crystal X-ray diffraction (SC-XRD). The crystals were obtained by layering fullerene solutions in CS_2 (for **Dy₂C₂-I**) or toluene (other EMFs) with a benzene solution of nickel octaethylporphyrin (NiOEP) in glass tubes. After slow diffusion of solutions during 3–4 weeks, fullerene-NiOEP co-crystals were obtained as black blocks on the tube walls. X-ray diffraction data collection was carried out at 100 K using synchrotron irradiation at the BESSY storage ring (BL14.2, Berlin-Adlershof, Germany).⁴¹ XDSAPP2.0 suite was employed for data processing.^{42,43} The structures were solved by direct methods and refined by SHELXL-2018.⁴⁴ Hydrogen atoms were added geometrically and refined with a riding model. In each structure, the fullerene molecule is supported by one NiOEP molecule, which is the typical packing character of fullerene-NiOEP co-crystals.^{45–47} The endohedral units showed a considerable disorder as is common in EMF crystallography. However, in all crystals we could identify one major site with enhanced occupancy, which allowed discussion of the cluster shape and internal position inside the fullerene if not precise geometry parameters. Additional crystal data can be found in ESI† (Table S1 and Fig. S7, S8).

Table 1 DFT (PBE/TZ2P) stability row of C_{88}^{4-} isomers and corresponding EMF structures

Isomer	C_{88}^{4-}		$\text{Y}_2\text{O}@C_{88}$		$\text{Y}_2\text{C}_2@C_{88}$		Known structures	This work
	ΔE (kJ mol ⁻¹)	Gap (eV)	ΔE (kJ mol ⁻¹)	Gap (eV)	ΔE (kJ mol ⁻¹)	Gap (eV)		
$D_2(35)$	0.0	0.59	0.0	0.75	0.0	0.75	Sm_2 , ³⁰ Lu_2C_2 ³¹	Dy_2O , Dy_2C_2
$C_s(32)$	30.2	0.46	16.5	0.69	13.2	0.69	Er_2C_2 , ³⁴ Lu_2C_2 ³¹	Dy_2O , Dy_2C_2
$C_1(26)$	28.6	0.69	21.1	0.87	38.5	0.84	Y_2C_2 , ³³ Lu_2 ³¹	Dy_2O
$C_1(30)$	47.7	0.40	36.2	0.59	30.0	0.63		
$C_s(\text{hept})$	67.0	0.64	54.0	0.77	57.7	0.79	Sc_2C_2 , ³² Lu_2C_2 ³⁵	



Dy₂O-I (Dy₂O@C₁(26)-C₈₈). The asymmetric unit contains half NiOEP molecule, two halves of fullerene molecule with 0.5 occupancies, half benzene molecule and two halves of toluene molecule with 0.5 occupancies. The intact NiOEP molecule is generated from the half NiOEP molecule with its image by the crystal mirror plane, which coincides with the NiOEP molecule's mirror symmetry plane. The two halves of the fullerene cage and their images by the crystal mirror plane are correlated by the crystal mirror plane as two enantiomers of the chiral C₁(26)-C₈₈ fullerene cage (Fig. 1a). The encapsulated Dy₂O cluster is disordered, however with high occupancies of 0.35 and 0.40 (out of 0.50) for the two main metal sites. The occupancies of the four remaining minor sites are 0.03–0.09 (Fig. 1a). The main site has Dy–O bond lengths of 2.019(4) and 2.050(4) Å, the Dy₁–O–Dy₂ angle of 166.0(2)°, and Dy₁⋯Dy₂ distance of 4.0386(9) Å.

Dy₂C₂-I (Dy₂C₂@C_s(32)-C₈₈). The asymmetric unit contains one intact NiOEP molecule, one intact fullerene molecule, one ordered benzene molecule and a disordered solvent molecule. The ordered fullerene cage is assigned as C_s(32)-C₈₈. The encapsulated Dy₂C₂ cluster is considerably disordered with 11 Dy sites, which are grouped into two regions with net occupancy of 1 in each of them. The main Dy sites in each group, Dy₁ (0.60) and Dy₂ (0.34)/Dy₁₀ (0.31), have sufficiently high occupancy to allow the discussion of the cluster geometry. The C₂ unit is refined as ordered, with the C–C bond length of 1.20(2) Å. In the main sites, the Dy₂C₂ cluster has a butterfly shape, in which Dy₁–C distances are 2.48(2) and 2.49(2), the angle between two Dy–C₂ planes is 150°, and the Dy⋯Dy distances are 4.54(2) Å (Dy₁⋯Dy₂), and 4.47(2) Å (Dy₁⋯Dy₁₀).

Dy₂C₂-II (Dy₂C₂@D₂(35)-C₈₈) and Dy₂O-III (Dy₂O@D₂(35)-C₈₈). The fullerene-NiOEP·2C₇H₈ crystals of both compounds are essentially isostructural. The asymmetric unit contains one half NiOEP molecule with unit site occupancy, two halves of fullerene molecule in half (0.5) site occupancy, and two disordered toluene molecules. The fullerene cage is assigned to the D₂(35)-C₈₈ isomer. Positions of its two enantiomers related by the crystallographic mirror symmetry plane overlap, resulting in the overall carbon cage disorder.

Positions of endohedral clusters inside the fullerene are also very similar in the two structures. Dy atoms are disordered, but show enhanced occupancies of 0.28/0.34 (out of 0.50) for the main metal sites, which are located on one of the two-fold axes of the D₂-symmetric fullerene cage. In Dy₂C₂@D₂(35)-C₈₈, the C₂ unit has the bond length of 1.23(1) Å, and the main site of the Dy₂C₂ cluster has a slightly bent butterfly shape, with Dy–C bond lengths of 2.401(6), 2.393(6), 2.417(6), and 2.433(7) Å, the angle between Dy₁–C₂ and Dy₂–C₂ planes of 161.4(4)°, and Dy₁⋯Dy₂ distance of 4.602(2) Å. In Dy₂O@D₂(35)-C₈₈, Dy–O bond lengths in the main site are 2.061(3) and 2.109(3) Å, the Dy₁–O–Dy₂ angle is 173.9(2)°, and Dy₁⋯Dy₂ distance is 4.164(2) Å.

DFT calculations

Crystallographic studies were augmented by extensive DFT calculations of Y₂O@C₈₈ and Y₂C₂@C₈₈ for the four lowest-energy C₈₈⁴⁻ isomers, including D₂(35), C_s(32), C₁(26), and C₁(30), and also for C_s(hept), which was earlier found in some C₈₈-based EMFs.^{32,35} For each cage isomer, we first used Fibonacci sampling to generate 120 starting structures with different orientations of the Y₂O endohedral cluster^{27,48} and then per-



Fig. 1 SC-XRD structures of Dy-EMFs co-crystallized with NiOEP. (a) Dy₂O-C₁(26); (b) Dy₂C₂-C_s(32); (c) Dy₂C₂-D₂(35); (d) Dy₂O-D₂(35). In each figure, coordination of the fullerene with the major site of the endohedral cluster to NiOEP is shown on the left, whereas all metal sites in endohedral clusters with their site occupancies and selected geometrical parameters are shown on the right. Note that in (a), (c), and (d), only one from two overlapping fullerene enantiomers is shown.



formed their complete optimization, which gave several unique conformers (Fig. S9†). For $Y_2C_2@C_{88}$, the reduced set of starting coordinates based on $Y_2O@C_{88}$ conformers was used, in which oxygen atom was replaced by the acetylide group. Relative energies of the most stable conformers for each cage isomer are listed in Table 1, more detailed data can be found in ESI.† The conformers of $Y_2O@C_{88}$ and $Y_2C_2@C_{88}$ were then re-optimized with Dy replacing Y (Fig. 2). Since Y^{3+} and Dy^{3+} have similar ionic radii, the structure and relative energies are very similar, and the following discussion is based on Y analogs.

The most stable isomers of C_{88}^{4-} , $Y_2O@C_{88}$, and $Y_2C_2@C_{88}$ all have the $D_2(35)-C_{88}$ cage. For $Y_2O@C_{88}$, the calculations revealed only four unique conformers, of which two are 34 kJ mol^{-1} higher in energy than the two most stable ones. The structure of the lowest-energy conformer corresponds to the main site in SC-XRD structures of $Dy_2O-D_2(35)$ and $Dy_2C_2-D_2(35)$ with the metal atoms aligned along the C_2 axis of the cage. The Y_2O cluster in this conformer is linear, but attains the Y–O–Y angles of 166° and 155° in higher-energy conformers. Likewise, the Y_2C_2 cluster is planar in the most stable conformer of $Y_2C_2@D_2(35)-C_{88}$. Interestingly, the optimized Y...Y distance in $Y_2O@C_{88}$ is 0.436 Å shorter than in $Y_2C_2@C_{88}$ (4.206 Å versus 4.642 Å; compare to experimental values of 4.164(2) Å and 4.602(2) Å in Dy analogs), which leads to the shorter distance between the metal and the coordinated hexagon in $Y_2C_2@C_{88}$ (2.015 Å) than in $Y_2O@C_{88}$ (2.167 Å) and makes the fullerene cage in $Y_2C_2@C_{88}$ longer by 0.133 Å (8.673 Å versus 8.540 Å measured as the distance between centroids of Y-coordinated hexagons). A considerable variation of the fullerene size depending on the endohedral species was observed earlier in $La_2@D_5(450)-C_{100}$ compared to $La_2C_2@D_5(450)-C_{100}$, but in that case it was the carbide cluster-fullerene which had the shorter length, whereas the La–C₆ distance was identical in both structures, and the whole effect

could be explained by a stronger Coulomb repulsion between La ions when not mediated by the acetylide group.⁴⁹

The next in the stability row are $Y_2O@C_{88}$ and $Y_2C_2@C_{88}$ isomers based on the $C_s(32)-C_{88}$ cage. The conformer survey of $Y_2O@C_s(32)-C_{88}$ gave 6 unique structures, of them three are almost isoenergetic within 4 kJ mol^{-1} and separated from other conformers by a gap of 25 kJ mol^{-1} . The Y_2O/Dy_2O cluster in all of them is nearly linear with the M–O–M angle of $174\text{--}179^\circ$. For $Y_2C_2@C_s(32)-C_{88}$, the lowest-energy conformer has the same position of metal atoms as in the most stable conformer of $Y_2O@C_{88}$ and corresponds to the main site in the SC-XRD structure of $Dy_2C_2-C_s(32)$ and $Lu_2C_2@C_s(32)-C_{88}$.³¹ The cluster is planar and is located on the symmetry plane of the fullerene cage.

$Y_2O@C_1(26)-C_{88}$ is found to be the third most stable isomer of $Y_2O@C_{88}$. The endohedral cluster is located rather freely, with 9 unique conformers spread in the energy range of 57 kJ mol^{-1} , of which six fall into the window of 15 kJ mol^{-1} . The major site in the SC-XRD structure of $Dy_2O-C_1(26)$ corresponds to the second conformer with the relative energy of 1.1 kJ mol^{-1} . The Y–O–Y angle in this structure is 157° , but the Y_2O cluster appears to be rather flexible with the angle varying strongly between conformers.

To summarize, the cage structures identified in this work for $Dy_2O@C_{88}$ and $Dy_2C_2@C_{88}$ by SC-XRD correspond to the most stable cage isomers, whereas locations of the endohedral cluster, at least in their major crystallographic sites, correspond to the lowest-energy conformers. The disorder in the crystal structures may be partially caused by the conformational freedom as DFT predicts several structures with close energies. The relative energies of $C_1(30)$ and $C_s(\text{hept})$ isomers are not prohibitively high, and their formation should be considered as plausible, although they were not found in this work. A deeper study of other cage isomers and their thermo-

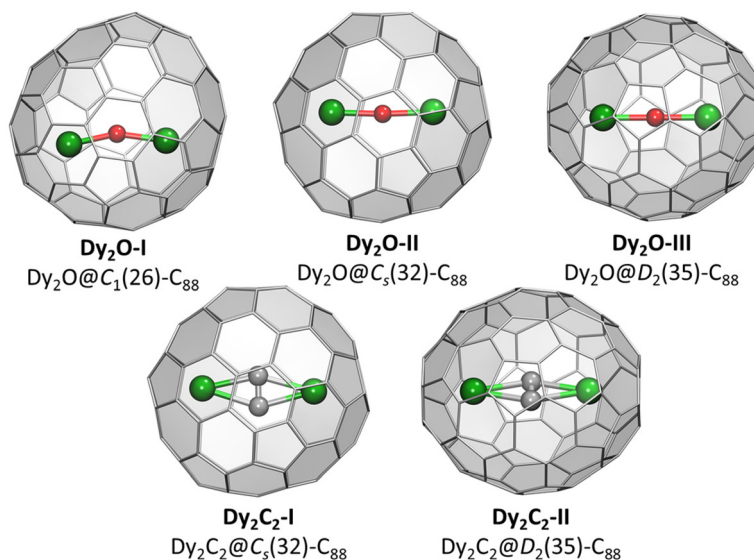


Fig. 2 DFT-optimized molecular structure of Dy-EMFs (the lowest-energy conformers). Dy – green, O – red, C – gray.



dynamic functions may be required to fully disclose the stability row, but this exercise goes beyond the scope of this work.

Spectroscopic properties

While the SC-XRD is the golden standard of the molecular structure determination, a disorder may pose a serious problem for the structure elucidation and even reduce the reliability of the fullerene isomer assignment of EMFs. The high structural sensitivity of UV-Vis-NIR absorption spectra makes them a convenient complimentary technique, which can help resolving questionable structural assignments. If endohedral clusters are not contributing to the frontier orbitals, the absorption spectra of EMFs are dominated by $\pi \rightarrow \pi^*$ excitations of the carbon cage. As a result, the spectra of EMFs with different metals or even different types of endohedral clusters may be very similar when they have the same fullerene isomer in the same formal charge state. In particular, close similarity of the spectra can be expected for the same isomers of carbide and oxide clusterfullerenes, as well as of dimetallofullerenes with divalent metals, as they all share the formal fullerene charge of 4-. The exact similarity, however, is expected only if the cluster is not involved at all, which is often not the case. Thus, different positions of the endohedral metal atoms (*i.e.* different conformers) may also contribute to the distinctions between the spectra.

Fig. 3 compares UV-Vis-NIR absorption spectra of Dy-EMFs isolated in this work. The spectrum of $\text{Dy}_2\text{O}-\text{C}_1(26)$ with $\text{C}_1(26)-\text{C}_{88}$ cage resembles the spectra reported for $\text{Y}_2\text{C}_2@-\text{C}_1(26)-\text{C}_{88}$ ³³ and $\text{Lu}_2@-\text{C}_1(26)-\text{C}_{88}$,³¹ but also that of $\text{Er}_2\text{C}_2@-\text{C}_s(32)-\text{C}_{88}$ from ref. 34. Given that the latter is also different from the spectra of other EMFs with $\text{C}_s(32)-\text{C}_{88}$ cage, we suggest that the $\text{Er}_2\text{C}_2@-\text{C}_{88}$ identified as the $\text{C}_s(32)$ isomer in ref. 34 requires reassignment to $\text{C}_1(26)$.

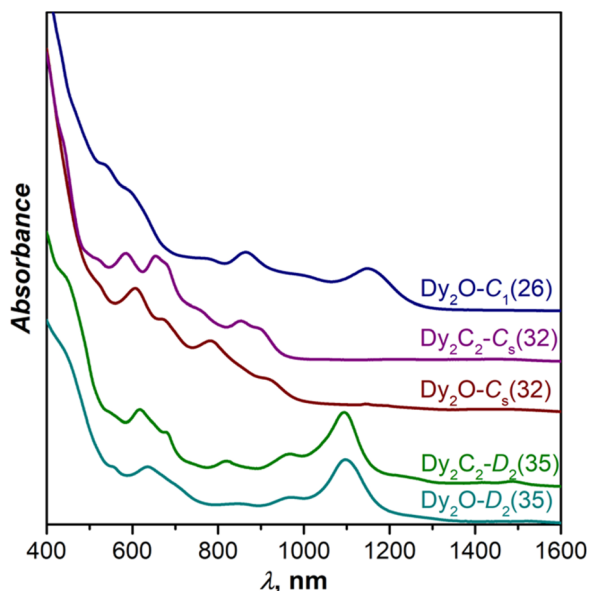


Fig. 3 Vis-NIR absorption spectra of $\text{Dy}_2\text{O}@-\text{C}_{88}$ and $\text{Dy}_2\text{C}_2@-\text{C}_{88}$ isomers measured in toluene solution at room temperature.

The spectrum of $\text{Dy}_2\text{C}_2-\text{C}_s(32)$ is virtually identical to that of $\text{Lu}_2\text{C}_2@-\text{C}_s(32)-\text{C}_{88}$ from ref. 31, in agreement with the same fullerene cage determined by SC-XRD for both structures. It also shows a certain similarity to the spectrum of $\text{Dy}_2\text{O}-\text{II}$, the only compound for which we did not succeed with the SC-XRD structure elucidation. We thus tentatively assign $\text{C}_s(32)$ isomer to $\text{Dy}_2\text{O}-\text{II}$, and further confirm this assignment by IR spectroscopy as discussed below.

In line with the same cage isomerism and metal positions determined by SC-XRD, $\text{Dy}_2\text{C}_2-\text{D}_2(35)$ and $\text{Dy}_2\text{O}-\text{D}_2(35)$ have almost identical absorption spectra. Comparison to the literature data gave rather puzzling results. Our spectra are similar to that of $\text{Sm}_2@-\text{C}_{88}-\text{D}_2(35)$ ³⁰ with the same fullerene cage as determined in this work, but also show a close resemblance with the spectra of $\text{Sc}_2\text{C}_2@-\text{C}_s(\text{hept})-\text{C}_{88}$ ³² and $\text{Lu}_2\text{C}_2@-\text{C}_s(\text{hept})-\text{C}_{88}$.³⁵ We thus decided to look for further spectroscopic verification of the fullerene cage structure.

IR spectra are also very sensitive to the molecular structure of the fullerene cage. Besides, they can be predicted by DFT with high accuracy. This good agreement between experiment and theory was used earlier for the correct determination of some EMF structures when SC-XRD data were not available yet.⁵⁰⁻⁵² Fig. 4a compares experimental and calculated spectra of $\text{Dy}_2\text{C}_2-\text{C}_s(32)$ and $\text{Dy}_2\text{O}-\text{C}_s(32)$ (note that calculations were performed for Y analogs, which does not affect the results of comparison because metal-based modes occur at much lower frequencies). For $\text{Dy}_2\text{C}_2-\text{C}_s(32)$, the theory gives very good agreement with the experiment, especially in the range of tangential fullerene modes above 1000 cm^{-1} . For $\text{Dy}_2\text{O}-\text{C}_s(32)$, we averaged the spectra of three low-energy conformers, as their spectra were found to be rather different. After the averaging, reasonable agreement with experimental data was obtained. Note that the spectra of $\text{Dy}_2\text{C}_2-\text{C}_s(32)$ and $\text{Dy}_2\text{O}-\text{C}_s(32)$ with the same fullerene cage are still considerably different, which shows that the internal cluster and position of metal atoms do affect the IR spectra. Earlier we have already seen similar differences in the spectra of EMFs with $I_h-\text{C}_{80}$ fullerene cage and different endohedral units.⁵³

For $\text{Dy}_2\text{C}_2-\text{D}_2(35)$ (Fig. 4b) and $\text{Dy}_2\text{O}-\text{D}_2(35)$ (Fig. 4c), the calculated spectra of $\text{D}_2(35)$ isomers show strikingly good agreement with the experimental data, whereas those of $\text{C}_s(\text{hept})$ isomers are substantially different. Thus, the IR spectroscopy confirms the cage isomer assignment of $\text{Dy}_2\text{C}_2-\text{D}_2(35)$ and $\text{Dy}_2\text{O}-\text{D}_2(35)$. Both EMFs have a very characteristic absorption band at 1574 cm^{-1} with a particularly strong intensity considerably exceeding that of all other absorption features. DFT calculations ascribe this band to the stretching vibration of the shortest C=C bonds in the molecule (1.384 \AA) located between pentagons in four pyracylene fragments.

Magnetic properties

The isolation of three isomers of $\text{Dy}_2\text{O}@-\text{C}_{88}$ and two isomers of $\text{Dy}_2\text{C}_2@-\text{C}_{88}$ allows us to analyze how the structural peculiarities of endohedral clusters and fullerene cages can



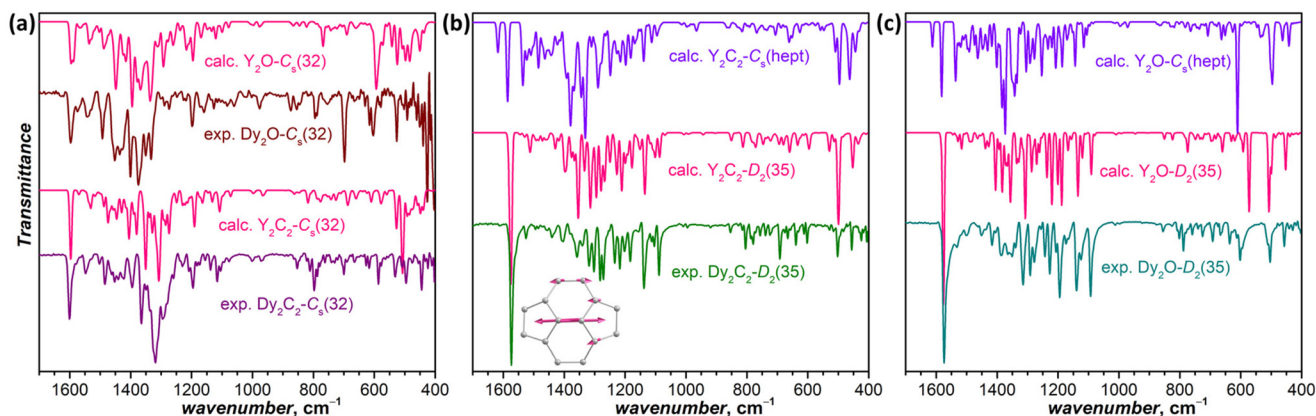


Fig. 4 Experimental and DFT-computed IR spectra: (a) $\text{Dy}_2\text{O}-\text{C}_5(32)$ and $\text{Dy}_2\text{C}_2-\text{C}_5(32)$; (b) $\text{Dy}_2\text{C}_2-\text{D}_2(35)$; (c) $\text{Dy}_2\text{O}-\text{D}_2(35)$. Computations are performed for Y analogs. The inset in (b) shows vibrational displacements of pyracylene fragment responsible for the strong band at 1574 cm^{-1} .

affect the magnetic properties of Dy EMFs. The first effect may be addressed by comparing isostructural Dy_2O and Dy_2C_2 compounds, whereas the second one can be considered by comparing different cage isomers with the same endohedral cluster. The role of the non-metal units, such as O^{2-} and C_2^{2-} , in the magnetism of EMFs is two-fold: they have a strong influence on the single-ion magnetic anisotropy of Dy ions by providing the main contribution to the ligand field,^{54–58} and they play a role of bridges between two Dy ions thus determining the strength of superexchange interactions.^{25,27,57,59–61}

Ab initio calculations

The single-ion anisotropy can be analyzed straightforwardly through multiconfigurational *ab initio* methods, such as the CASSCF/RASSI approach in Molcas employed in this work.^{62,63} We use $\text{Dy}_2\text{O}-\text{D}_2(35)$ and $\text{Dy}_2\text{C}_2-\text{D}_2(35)$ as representative

examples as they have the same fullerene cage isomer and identical η^6 -coordination of Dy ion to the carbon cage, and hence the difference between them can be directly ascribed to the different influence of O^{2-} and C_2^{2-} units. Fig. 5 shows the calculated ligand field splitting and orientation of magnetic moments for Dy ions in $\text{Dy}_2\text{O}-\text{D}_2(35)$ and $\text{Dy}_2\text{C}_2-\text{D}_2(35)$. Both O^{2-} and C_2^{2-} impose an axial ligand field on Dy ions, yielding the ground state Kramers doublet (KD) with $J_z = \pm 15/2$. The orientation of the quantization axis is also similar in both clusters as it coincides with Dy–O bond in Dy_2O and passes through the center of the acetylide group in Dy_2C_2 . However, the ligand-field splitting and the degree of axiality imposed by O^{2-} and C_2^{2-} are very different. On average, the splitting in Dy_2O is twice higher than in Dy_2C_2 (481 cm^{-1} versus 224 cm^{-1} for the first excited KD and 1494 cm^{-1} versus 780 cm^{-1} for the whole LF splitting in the ground-state ${}^6H_{15/2}$ multiplet).

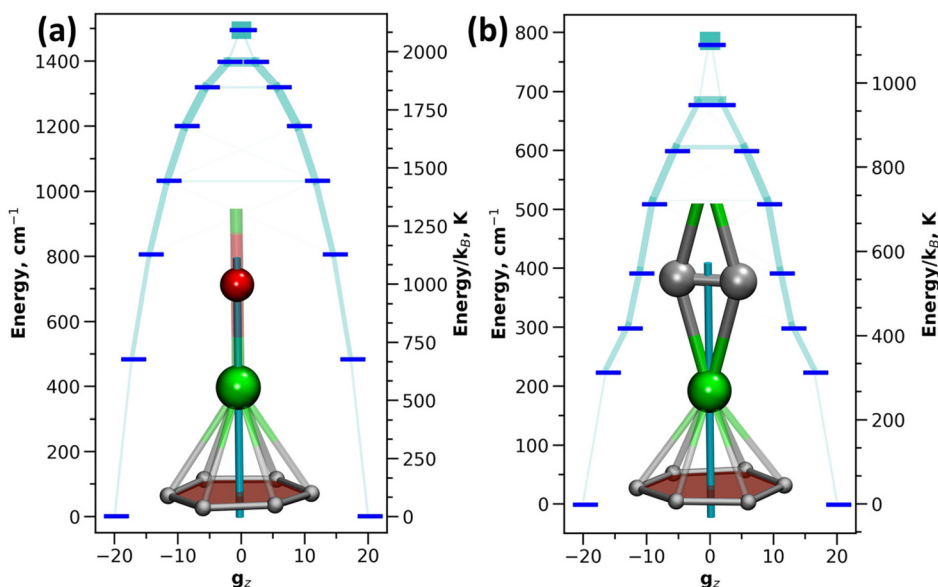


Fig. 5 Ligand-field splitting in Dy ions in $\text{Dy}_2\text{O}-\text{D}_2(35)$ (a) and $\text{Dy}_2\text{C}_2-\text{D}_2(35)$ (b) computed at the CASSCF/RASSI level. Insets show fragments of the molecules with atoms surrounding Dy ions. Quantization axes are shown in light blue, Dy – green, O – red, C – gray.



Already for the ground-state KD, the g_x and g_y components of the pseudospin g -tensor in $\text{Dy}_2\text{C}_2@C_{88}$ are 50 times larger than in $\text{Dy}_2\text{O}@C_{88}$. This indicates that Dy magnetic moments in Dy_2C_2 are more susceptible to perturbations of the magnetic field and hence can relax faster. A purity of the KD states when presented in $|m_j\rangle$ basis is also considerably higher in Dy_2O than in Dy_2C_2 . In the latter, only the first KD is relatively pure with 99.8% of the $|15/2\rangle$ term, whereas already in the second KD the contribution of the leading $|13/2\rangle$ term is only 86.5%, and the mixing is further increased in higher-energy KDs. In $\text{Dy}_2\text{O}@C_{88}$, the leading term contributions in the four lowest-energy KDs are 100.0% $|15/2\rangle$, 99.9% $|13/2\rangle$, 97.7% $|11/2\rangle$, and 94.3% $|9/2\rangle$, and only in the fifth KD the weight decreases below 90%, to 89.2% for $|7/2\rangle$. Thus, the Dy_2O cluster with the negative charge localized on the single oxide ion features much stronger axially than the Dy_2C_2 cluster, in which the negative charge is spread over two carbons.

SQUID magnetometry

As follows from the results of *ab initio* calculations, magnetic ground state of Dy ions in all the studied EMFs is the Ising state with $J_z = \pm 15/2$. It means that the differences in the static low-temperature magnetic behavior of the compounds should be caused by variation in the Dy...Dy interactions. The latter can be conveniently addressed by measurements of the temperature dependence of the magnetic susceptibility χ as the shape of the χT product curve exhibits characteristic signatures of interactions between magnetic moments. For two non-interacting moments, the curve should be almost flat with a steep decrease at the lowest temperatures. This is the behavior we observe for $\text{Dy}_2\text{O}-C_s(32)$ (Fig. 6). For the antiferromagnetic (AFM) coupling, the decrease of χT starts at higher temperatures and is smoother, which corresponds to the behavior

found for $\text{Dy}_2\text{O}-C_1(26)$. Finally, for the ferromagnetically-coupled (FM) moments, the χT curve develops a peak at low temperatures, which matches the behavior of $\text{Dy}_2\text{O}-D_2(35)$. Thus, from the χT measurements, we infer that the isomers of $\text{Dy}_2\text{O}@C_{88}$ represent three different situations of magnetic Dy...Dy interactions. For the $\text{Dy}_2\text{C}_2@C_{88}$ isomers the situation is different – both $\text{Dy}_2\text{C}_2-C_s(32)$ and $\text{Dy}_2\text{C}_2-D_2(35)$ show clear signatures of FM coupling, which is stronger in $\text{Dy}_2\text{C}_2-C_s(32)$. For all the compounds, the shapes of experimental χT curves are well reproduced by simulations with interaction parameters determined from the fit of magnetization curves as described below.

Further details are obtained from isothermal magnetization curves plotted in Fig. 7. All three $\text{Dy}_2\text{O}@C_{88}$ isomers show magnetic hysteresis with a closing temperature of around 8–9 K at a sweep rate of 2.9 mT s⁻¹. The hysteresis closing temperature matches the bifurcation temperatures of χ curves measured in zero-field cooled sample (ZFC) and during the in-field cooling (FC) and listed in Table 2 (see also insets in Fig. 7).

The shapes of hysteresis are quite different between the isomers and reflect the nature of Dy...Dy interactions deduced from χT measurements. The most distinctive are the curves measured for $\text{Dy}_2\text{O}-C_1(26)$. At 1.8 K the hysteresis is open in the whole measurement range from -7 T to +7 T and clearly shows two regimes with a small and large magnetic moment. The low-field regime corresponds to the dominant AFM alignment of the magnetic moments. But when the magnetic field exceeds 2 T, the state with the FM alignment gains lower energy and starts to increase its population, hence causing an increase of the magnetization. This hysteresis shape resembles that found in some other dinuclear Dy complexes with antiferromagnetic coupling,^{27,64–71} but the transition between the two states in $\text{Dy}_2\text{O}-C_1(26)$ occurs at a considerably higher field, pointing to a much stronger Dy...Dy coupling in the fullerene.

To obtain the numerical parameters of the coupling, we fitted magnetization curves measured at different temperatures using the effective spin Hamiltonian (1):

$$\hat{H}_{\text{spin}} = \hat{H}_{\text{LF}_1} + \hat{H}_{\text{LF}_2} - 2j_{12}\hat{J}_1 \cdot \hat{J}_2 + \hat{H}_{\text{ZEE}} \quad (1)$$

where \hat{H}_{LF_i} are single-ion ligand-field Hamiltonians of Dy^{3+} , j_{12} is the coupling constant between dysprosium moments, and \hat{H}_{ZEE} is the Zeeman term describing interaction of Dy^{3+} magnetic moments with the external magnetic field. We use *ab initio* computed ligand field parameters in \hat{H}_{LF_i} , and Dy^{3+} moments \hat{J}_i are treated in the $|J, m_j\rangle$ basis sets of the ${}^6H_{15/2}$ multiplet. In the lowest-energy part of the spectrum, the Hamiltonian yields two quasi-doublets associated with ferromagnetic and antiferromagnetic alignment of Dy^{3+} magnetic moments (Fig. S12 in ESI†). The energy difference between them depends on the coupling constant and the angle α between quantization axes of Dy^{3+} ions: $\Delta E_{\text{AFM-FM}} = 225j_{12} \cos(\alpha)$, where the coefficient 225 appears because of the use of the full Dy^{3+} momentum in the Hamiltonian (1) and the single-ion ground state with $J_z = \pm 15/2$ (see ESI† for more details). In the

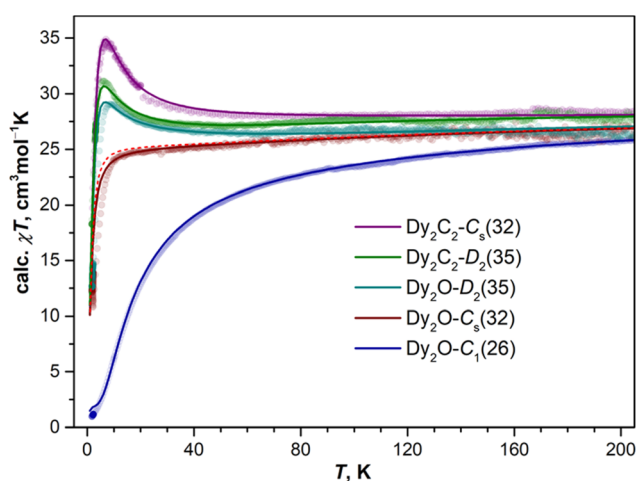


Fig. 6 Experimental χT curves (dots) and results of simulations (solid lines; red dashed line is calculated for the system of two non-interacting Dy ions) of Dy_2O and Dy_2C_2 EMFs with C_{88} cages. Magnetic susceptibility is defined as $\chi = M/H$ at 0.5 T. Experimental curves are corrected for linear background and scaled to match simulated curves in high-temperature range.



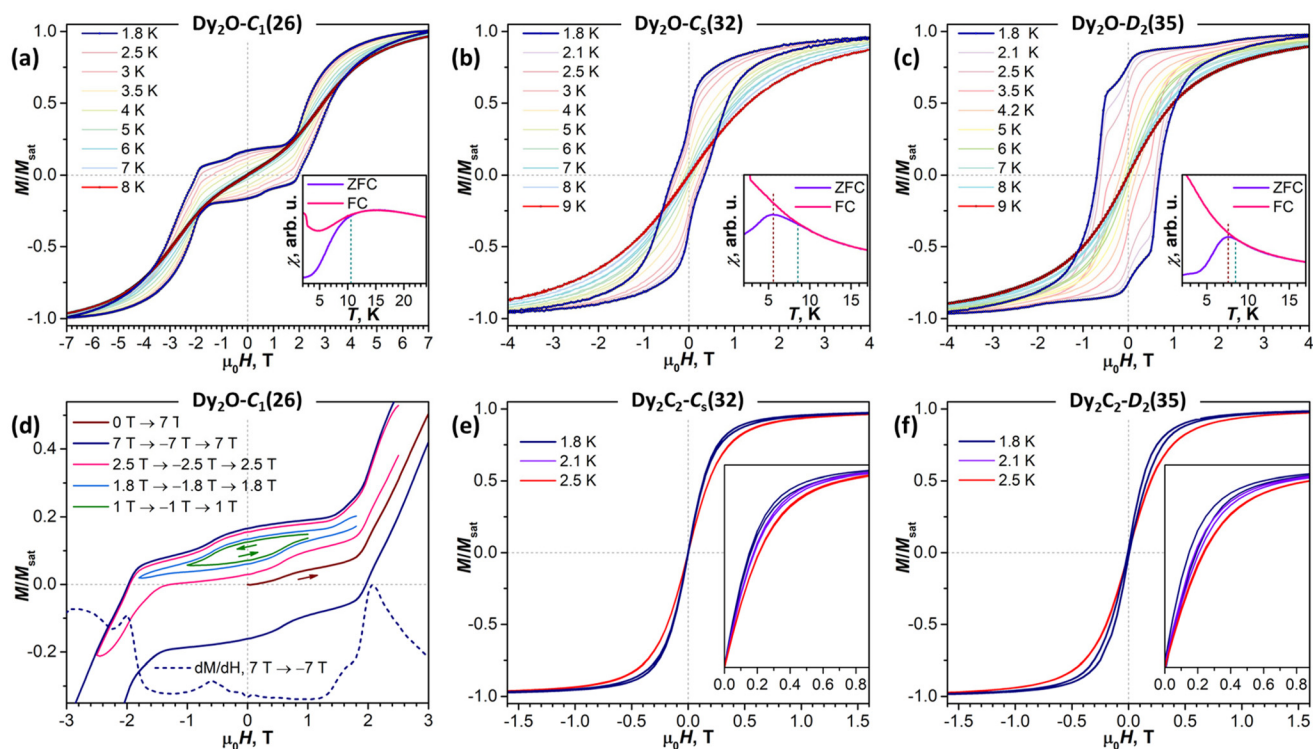


Fig. 7 Low-temperature magnetization curves of Dy₂O@C₈₈ and Dy₂C₂@C₈₈ EMFs: Dy₂O-C₁(26) (a and d), Dy₂O-C_s(32) (b), Dy₂O-D₂(35) (c), Dy₂C₂-C_s(32) (e), and Dy₂C₂-D₂(35) (f), sweep rate 2.9 mT s⁻¹. Insets in (a)–(c) show χ_{FC} and χ_{ZFC} curves (0.2 T, sweep rate 5 K min⁻¹) and determination of T_B and T_{irrev} . (d) Shows magnetic hysteresis of Dy₂O-C₁(26) measured in different field ranges at 1.8 K, as well as the derivative of the magnetization curve.

Table 2 Parameters of Dy...Dy interactions and magnetic hysteresis in Dy₂O@C₈₈ and Dy₂C₂@C₈₈ EMFs^{a,b}

	$\Delta E_{\text{AFM-FM}}$	j	α (°)	T_B	T_{irrev}	T_{hyst}	T_{B100}
Dy ₂ O-C ₁ (26)	-16.5	-0.080	23 ± 1		10.5	8	6.0
Dy ₂ O-C _s (32)	-0.4	-0.002	23 ± 11	5.5	8.5	8	4.6 (0.2 T)
Dy ₂ O-D ₂ (35)	3.6	0.022	43 ± 2	7.5	8.5	8	3.9
Dy ₂ C ₂ -C _s (32)	6.3	0.029	11 ± 3			2.1	
Dy ₂ C ₂ -D ₂ (35)	3.3	0.015	0 ± 5			2.1	

^a $\Delta E_{\text{AFM-FM}}$ (cm⁻¹), j (cm⁻¹), and α (°) are determined from the fits of magnetization curves. ^b T_B is defined as the peak temperature in χ_{ZFC} , T_{irrev} is the bifurcation point between χ_{ZFC} and χ_{FC} curves (both measured with the sweep rate 5 K min⁻¹), T_{hyst} is the highest temperature at which the hysteresis loop is still open (sweep rate 2.9 mT s⁻¹), and T_{B100} is the temperature, at which magnetization relaxation time is 100 s; all temperatures are in K.

fitting with PHI code,⁷² j_{12} and α were treated as free parameters, and computed curves were powder-averaged to be compatible with experimental magnetization curves measured for powder samples. Finally, only experimental points in the field range where hysteresis is very narrow or completely closed were used as the Hamiltonian (1) does not include relaxation processes and hence cannot be used to model magnetic hysteresis. Experimental and fitted magnetization curves are compared in ESI.† Although different conformers of EMF molecules may have somewhat different single-ion LF parameters and LF splitting, our calculations in this work as well as earlier studies^{25–27,57} showed that the ground state KD of Dy ions in such EMFs are very close to the pure $m_J = \pm 15/2$ state irrespective of the Dy-cage coordination. Furthermore, the energy gap

to the first excited KD is so high that only the ground-state KD will have significant population at low temperatures. Thus, it is not expected that the results of simulations with eqn (1) will be noticeably affected by the coexistence of different orientations of endohedral clusters or by accuracy limitations of the *ab initio* modelling of the LF splitting.

For Dy₂O-C₁(26), the fitting procedure gave α of 23 ± 1° and j_{12} of -0.08 cm⁻¹, yielding the $\Delta E_{\text{AFM-FM}}$ value of -16.5 cm⁻¹, one of the largest interaction energies between Dy magnetic moments in dinuclear {Dy₂} compounds (see ref. 27 for a recent survey). Note that since Dy³⁺ magnetic moments in the Dy₂O-C₁(26) molecule are not collinear, the magnetic moment of the ground AFM state is not zero but amounts to 20 sin($\alpha/2$) = 4 μ_B . The fitted parameters and Hamiltonian (1) were then



used to simulate χT curve, which gave good agreement to the experimental data (Fig. 6), thus confirming the reliable determination of the interaction parameters.

In $\text{Dy}_2\text{O}-\text{C}_s(32)$, the hysteresis shape features a considerable decrease of the magnetization near zero field, which is consistent with the weak Dy...Dy interactions. When the coupling is negligible, an additional magnetization relaxation channel *via* zero-field quantum tunneling of magnetization is open, which results in a drastically reduced remanence. This hysteretic behavior is similar to the recently studied $\text{Dy}_2\text{O}@C_{74}$,²⁵ although the QTM signatures in the hysteresis curve of $\text{Dy}_2\text{O}-\text{C}_s(32)$ are less pronounced than in the latter. The fitting of the magnetization curves with Hamiltonian (1) gave the angle of $23 \pm 11^\circ$ and a very small constant j_{12} of -0.002 cm^{-1} . Note that when the coupling is weak, the dependence of the curves on the angle between magnetic moment is also reduced, thus resulting in a larger uncertainty. The small $\Delta E_{\text{AFM-FM}}$ value of only -0.4 cm^{-1} is in line with the shape of χT curve, which is also well reproduced by simulations.

The shape of the magnetic hysteresis in $\text{Dy}_2\text{O}-\text{D}_2(35)$ resembled that observed for some other dinuclear lanthanide fullerenes with FM coupling, such as $\text{Dy}_2\text{ScN}@C_{80}$,⁷³ $\text{Tb}_2\text{ScN}@C_{80}$,⁷⁴ and $\text{Dy}_2\text{S}@C_{82}$.⁶¹ After the sample is saturated at 7 T, ramping the field down produces only a small decrease of magnetization until reaching zero field. On crossing zero field, a certain decrease of magnetization occurs, which is likely due to the zero-field QTM. But the latter implies simultaneous flip of magnetic moments of both Dy^{3+} ions, and is not very efficient in a strongly coupled system. At a further negative ramping, another kink in the curve is seen at -0.48 T , after which the magnetization drops abruptly. Following earlier studies,^{61,74,75} this feature is assigned to the level crossing between the FM and AFM states, which promotes the efficient relaxation of magnetization *via* the QTM mechanism. Fitting the magnetization curves of $\text{Dy}_2\text{O}-\text{D}_2(35)$ resulted in j_{12} of 0.022 cm^{-1} , α of $43 \pm 2^\circ$, and $\Delta E_{\text{AFM-FM}}$ of 3.6 cm^{-1} . The angle is unexpectedly large, given that SC-XRD and DFT results agree on the linear shape of the Dy_2O cluster. Yet these parameters also give a good match between simulated and experimental χT curves. The AFM-FM energy difference can be also estimated from the magnetic field of the QTM kink (H_{QTM}) in the hysteresis curve as $\Delta E_{\text{AFM-FM}} = 0.935 H_{\text{QTM}} [T] \mu_{\text{Dy}} [\mu_{\text{B}}]$ (ref. 61), which gives 4.4 cm^{-1} .

In both isomers of $\text{Dy}_2\text{C}_2@C_{88}$, only a very narrow opening of the hysteresis is observed at 1.8 K and 2.1 K, and the loop is completely closed by 2.5 K. Fitting of the magnetization curves gives the FM coupling with $\Delta E_{\text{AFM-FM}}$ of 6.3 cm^{-1} in $\text{Dy}_2\text{C}_2-\text{C}_s(32)$ and 3.3 cm^{-1} in $\text{Dy}_2\text{C}_2-\text{D}_2(35)$. The angle between magnetic moments is only $11 \pm 3^\circ$ in $\text{Dy}_2\text{C}_2-\text{C}_s(32)$ and is nearly 0° in $\text{Dy}_2\text{C}_2-\text{D}_2(35)$ within the uncertainty limit of $\pm 5^\circ$.

Magnetization relaxation times

The open magnetic hysteresis indicates that the studied Dy-EMFs are single-molecule magnets,⁷⁶⁻⁸⁰ and their magnetodynamics was further characterized by measuring the relaxation times τ_{M} at different temperatures. As the sample amount was

not sufficient for AC measurements, only DC technique was employed. The samples were first magnetized at the field of 7 T, then the field was ramped down to zero as fast as possible, and the decay of magnetization was then followed and fitted with a stretched exponential function. The values determined for $\text{Dy}_2\text{O}@C_{88}$ isomers are plotted in Arrhenius coordinates in Fig. 8. The DC technique is reliable only for relaxation times longer than 50–100 s, which limits the accessible temperature range to that below T_{B} .

For $\text{Dy}_2\text{O}-\text{C}_1(26)$, the increase of the relaxation time with cooling takes a linear form down to 2.5 K, with the sign of a leveling off at lower temperatures. The linear dependence is a characteristic feature of the Orbach relaxation mechanism with an effective barrier U^{eff} corresponding to an excited spin state:

$$\tau_{\text{M}}^{-1}(T) = \tau_0^{-1} \exp(-U^{\text{eff}}/T). \quad (2)$$

Fitting of the experimental data with eqn (2) gives U^{eff} of $20.5 \pm 0.3 \text{ K}$ (14.2 cm^{-1}) and the attempt time τ_0 of $3.3 \pm 0.3 \text{ s}$. The barrier is much smaller than the energies of excited LF states but is close to the $\Delta E_{\text{AFM-FM}}$ value determined from the fit of magnetization curves, which suggests that the magnetization reversal in the AFM ground state of $\text{Dy}_2\text{O}-\text{C}_1(26)$ proceeds *via* sequential flips of individual Dy magnetic moments, including a formation of the FM state after the first flip. The levelling off below 2.5 K may indicate the switch to the simultaneous flip of two Dy moments through a temperature-independent QTM such as observed in $\text{Dy}_2\text{S}@C_{82}$ at sub-K temperatures.⁶¹

In $\text{Dy}_2\text{O}-\text{C}_s(32)$, the measurement at zero field showed coexistence of the fast relaxation (presumably a QTM) with a slower thermal process, which makes a determination of τ_{M} rather ambiguous. As the zero-field QTM can be suppressed by

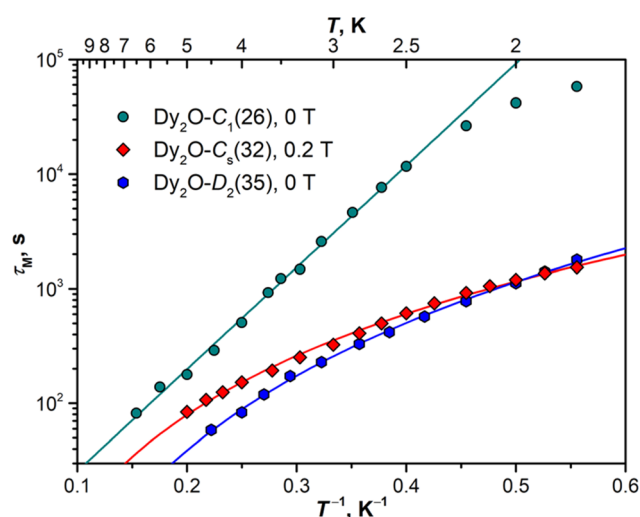


Fig. 8 Temperature dependence of the magnetization relaxation time measured for $\text{Dy}_2\text{O}@C_{88}$ isomers: $\text{Dy}_2\text{O}-\text{C}_1(26)$ (at 0 T), $\text{Dy}_2\text{O}-\text{C}_s(32)$ (0.2 T), and $\text{Dy}_2\text{O}-\text{D}_2(35)$ (0 T). Solid lines are fits with Orbach ($\text{Dy}_2\text{O}-\text{C}_1(26)$) and Raman mechanisms ($\text{Dy}_2\text{O}-\text{C}_s(32)$ and $\text{Dy}_2\text{O}-\text{D}_2(35)$).



application of a finite magnetic field, the measurements were then performed in the field of 0.2 T. For Dy₂O-D₂(35), the measurements were performed in zero field. Dy₂O-C_s(32) and Dy₂O-D₂(35) show a different temperature dependence of τ_M than Dy₂O-C₁(26), which can be described by a power-law function, $\tau_M^{-1}(T) = CT^n$, characteristic for the Raman relaxation mechanism. The fit gives similar parameters for two isomers, $C = (1.13 \pm 0.05) \times 10^{-4} \text{ s}^{-1} \text{ K}^{-n}$ and $n = 2.93 \pm 0.04$ in Dy₂O-C_s(32) and $C = (0.67 \pm 0.03) \times 10^{-4} \text{ s}^{-1} \text{ K}^{-n}$ and $n = 3.70 \pm 0.04$ in Dy₂O-D₂(35). The n values are much smaller than the classical expectation of $n = 9$ for the Raman process but are consistent with the behaviour of many other Dy-SMM, including Dy-EMFs, also showing smaller exponents in the Raman regime associated with the influence of optical phonons.⁸¹

For both Dy₂C₂@C₈₈ isomers, the relaxation times appeared too short for their reliable determination by DC magnetometry. Since an open magnetic hysteresis requires τ_M of at least a few seconds, a conservative estimation would be 5–10 seconds at 1.8 K. Much faster relaxation of magnetization in Dy₂C₂@C₈₈ when compared to Dy₂O@C₈₈ is in line with the *ab initio* calculations suggesting a substantially lower axiality in Dy₂C₂ clusters.

Discussion

With the study of Dy₂O@C₈₈ in this work, Dy-oxide clusterfullerenes Dy₂O@C_{2n} become the most diverse class of Dy-based EMF-SMMs both in terms of the cage size (ranging from C₇₂ to C₈₈) and isomeric composition (C₈₂ and C₈₈ are represented by three isomers each). Table 3 lists the energetic characteristics of Dy...Dy interactions and blocking temperatures of magnetization in the Dy₂O@C_{2n} series and compares the values to other dinuclear Dy-clusterfullerenes.

Our new results demonstrate that the O²⁻ bridge in Dy₂O cluster can support not only AFM interactions between Dy magnetic moments as in previously studied Dy₂O@C_{2n} EMFs, but also the FM coupling. It is different from Dy₂-clusterfullerenes with S²⁻, C₂²⁻, C⁴⁻, and N³⁻ bridges, which all favor the FM coupled ground state. Quite unusual is the magnitude of the variation of the Dy...Dy interaction energy found in seemingly similar Dy₂O@C₈₈ isomers. Estimation of dipolar contribution to $\Delta E_{\text{AFM-FM}}$ shows that $\Delta E_{\text{AFM-FM}}^{\text{dip}}$ is positive in all EMFs and falls into the energy range of 1.5–3 cm⁻¹. Thus, the exchange contribution to Dy...Dy coupling appears to be responsible for the strong variation of $\Delta E_{\text{AFM-FM}}$. Among the studied Dy₂O@C_{2n} compounds, only one, Dy₂O@D₂(35)-C₈₈, has moderately positive $\Delta E_{\text{AFM-FM}}^{\text{exch}}$ value of 1.4–2.2 cm⁻¹, whereas other 8 feature negative exchange term spanning from the modest -1.5 cm⁻¹ in Dy₂O@C₇₂ to very large -21.2 cm⁻¹ in Dy₂O@C₈₀ and -19.0 cm⁻¹ in Dy₂O@C₁(26)-C₈₈, by far the strongest Dy...Dy interactions in all Dy₂-complexes. The data does not present any clear correlation between the structural parameters and the strength of the exchange coupling. The fullerene cage definitively plays an important role, as can be deduced from the considerable variation of the values within the isomeric series, especially for isomers of Dy₂O@C₈₈. However, it is hard to conclude at this moment if this strong influence is caused by the variation of the Dy₂O cluster shape and size in different cages, by indirect interactions *via* the fullerene π -system, or because different Dy-fullerene coordination sites alter the metal orbital composition and hence modify the superexchange interactions *via* the O²⁻ bridge. A combined influence of all these factors is likely to play a role.

Comparison of different clusters within one fullerene cage can be used to distinguish the cage and the bridge effects. However, this also appears to be rather ambiguous. For instance, Dy₂C₂@D₂(35)-C₈₈ and Dy₂O@D₂(35)-C₈₈ have very close $\Delta E_{\text{AFM-FM}}$ values, but at the same time Dy₂C₂@C₈₈ and

Table 3 Dy...Dy interaction energy and blocking temperature of magnetization in dinuclear Dy-EMFs^a

	$\Delta E_{\text{AFM-FM}}^{\text{tot}}$	$\Delta E_{\text{AFM-FM}}^{\text{dip}}$	$\Delta E_{\text{AFM-FM}}^{\text{exch}}$	$U_{\text{exch}}^{\text{eff}}$	T_B	T_{irrev}	T_{B100}	Ref.
Dy ₂ O@C _s (10 528)-C ₇₂	1.5 ^b	3.0	-1.5	—	4.0	8	3.4	25
Dy ₂ O@C ₂ (13 333)-C ₇₄	~0.1 ^b	2.6	-2.5	—	6.7	14	5.0 (0.2 T)	25
Dy ₂ O@C _{2v} (5)-C ₈₀	-18.5 ^b	2.7	-21.2	18.0	5.0	11	3.2	26
Dy ₂ O@C _s (6)-C ₈₂	-7.5 ^c	3.0	-10.5	7.5	4.4	10	2.8	27
Dy ₂ O@C _{3v} (8)-C ₈₂	-5.4 ^c	2.5	-7.8	5.4	7.4	9	5.9	27
Dy ₂ O@C _{2v} (9)-C ₈₂	-12.9 ^c	2.6	-15.6	12.9	5.8	8	3.7	27
Dy ₂ O@C ₁ (26)-C ₈₈	-16.5 ^b	2.5	-19.0	14.2	—	10.5	6.0	Tw ^e
Dy ₂ O@C _s (32)-C ₈₈	-0.4 ^b	2.3	-2.7	—	5.5	8.5	4.6 (0.2 T)	Tw
Dy ₂ O@D ₂ (35)-C ₈₈	3.6 ^b /4.4 ^d	2.2	1.4/2.2	—	7.5	8.5	3.9	Tw
Dy ₂ C ₂ @C _s (6)-C ₈₂	12.1 ^c	2.6	9.5	12.1	~2	—	—	57
Dy ₂ C ₂ @C _s (32)-C ₈₈	6.3 ^b	1.7	4.6	—	~2	—	—	Tw
Dy ₂ C ₂ @D ₂ (35)-C ₈₈	3.3 ^b	1.7	1.6	—	~2	—	—	Tw
Dy ₂ S@C _s (6)-C ₈₂	11.0 ^b /10.7 ^d	2.2	8.5	12.4	~2	—	—	57 and 61
Dy ₂ S@C _{3v} (8)-C ₈₂	6.4 ^b /5.1 ^d	2.3	2.8	4.2	4.0	—	2.0	57 and 61
Dy ₂ TiC@I _h (7)-C ₈₀	8.5 ^b	3.4	5.1	6.6	~2	—	1.7	59 and 82
Dy ₂ ScN@I _h (7)-C ₈₀	5.6 ^c	3.3	2.3	5.6	7.9	8	5.0	56
Dy ₂ LuN@I _h (7)-C ₈₀	3.0 ^c	3.3	-0.3	3.0	7.9	10	5.2	60

^a $\Delta E_{\text{AFM-FM}}^{\text{exch}}$ is the difference of $\Delta E_{\text{AFM-FM}}^{\text{tot}}$ and $\Delta E_{\text{AFM-FM}}^{\text{dip}}$; $U_{\text{exch}}^{\text{eff}}$ is the energy barrier of the low-temperature Orbach process assigned to the relaxation *via* the exchange excitation; $\Delta E_{\text{AFM-FM}}$ and $U_{\text{exch}}^{\text{eff}}$ values in cm⁻¹, temperature in Kelvin. ^b $\Delta E_{\text{AFM-FM}}^{\text{tot}}$ is determined from the fit of magnetization curves. ^c $\Delta E_{\text{AFM-FM}}^{\text{tot}}$ is determined as the exchange barrier $U_{\text{exch}}^{\text{eff}}$. ^d $\Delta E_{\text{AFM-FM}}^{\text{tot}}$ is determined from the QTM features in hysteresis curves. ^e Tw - this work.



Dy₂O@C₈₈ isomers with the C_s(32) cage have different size and the sign of $\Delta E_{\text{AFM-FM}}$. The comparison of Dy₂O@C₈₂, Dy₂C₂@C₈₂, and Dy₂S@C₈₂ with C_s(6) cage isomer shows that the strength and the sign of Dy...Dy coupling in Dy₂S and Dy₂C₂ are similar, while Dy₂O counterpart has the opposite sign of $\Delta E_{\text{AFM-FM}}$ (Table 3). Finally, in isostructural and iso-electronic Dy₂TiC and Dy₂ScN clusters within the I_h(7)-C₈₀ cage, the superexchange through C⁴⁻ is almost twice stronger than through N³⁻.⁵⁹ Overall, we can conclude that the bridge is certainly crucial in determining the Dy...Dy coupling, but not in a very deterministic way as the influence of other factors may be of a comparable magnitude.

The SMM performance of Dy₂-clusterfullerenes does not show an obvious correlation with the Dy...Dy coupling strength but is clearly affected by the single-ion magnetic anisotropy. Thus, the blocking and hysteresis closing temperature in dinuclear systems reduces in the following row of the bridge units: O²⁻ > N³⁻ > C⁴⁻ > S²⁻ > C₂²⁻, which corresponds to the decrease of the average ligand-field splitting in these types of clusterfullerenes as predicted by *ab initio* calculations.^{54,55,57,59,83} Counterintuitively, this conclusion is not directly transferable to analogous mono-nuclear Dy-EMFs. The hysteresis closing temperature in DySc₂N@C₈₀,^{45,84} DyLu₂N@C₈₀,⁶⁰ DyY₂N@C₈₀,⁸⁵ DyScS@C₈₂,⁸⁶ and DyYTiC@C₈₀⁵⁸ is near 7–8 K irrespective of their non-metal units. The synthesis and studies of mixed-metal oxide and carbide clusterfullerenes with single Dy atom, such as DyScO@C₈₂ and DyScC₂@C₈₂, and the studies of mono-nuclear Dy-SMMs with different cage sizes will be required to fully disclose this phenomenon. However, it can be pointed out that the highest hysteresis closing temperature among Dy₂-clusterfullerenes, 14 K, is found for Dy₂O@C₇₄, in which the Dy...Dy coupling is so weak that the compound shows butterfly-shaped hysteresis with pronounced zero-field QTM typical for single-ion SMMs.²⁵

Although the Dy...Dy coupling does not seem to correlate with the blocking temperature in Dy₂-clusterfullerenes, it does affect the low-temperature relaxation. The distinct Orbach relaxation mechanism involving the exchange excitation (either FM → AFM or AFM → FM) is observed only in Dy₂-clusterfullerenes with $|\Delta E_{\text{AFM-FM}}|$ values exceeding a threshold of 5 cm⁻¹ (e.g., Dy₂O@C₁(26)-C₈₈). For compounds with weaker coupling, the relaxation is better described by the Raman mechanism (as Dy₂O@C_s(32)-C₈₈ and Dy₂O@D₂(35)-C₈₈, Fig. 8).

Conclusions

In this work, we report on the synthesis, isolation and systematic structural studies of endohedral metallofullerenes with Dy₂O and Dy₂C₂ clusters encapsulated within C₈₈ cages. As both clusters transfer four electrons to the fullerene host, they tend to feature the same cage isomers, which were identified by single-crystal X-ray diffraction as C₁(26), C_s(32), and D₂(35) and further supported by spectroscopic studies. These cage

isomers correspond to the most stable C₈₈⁴⁻ isomers according to DFT calculations.

The availability of isomeric and isostructural Dy₂O@C₈₈ and Dy₂C₂@C₈₈ EMFs allowed the study of magnetic Dy...Dy interactions as a function of the fullerene cage and the bridging unit. We showed that the oxide ion O²⁻ tends to prefer an antiferromagnetic coupling of Dy magnetic moments, whereas the acetylide group C₂²⁻ favors their ferromagnetic coupling. The strength of the interaction is found to vary strongly with the fullerene cage isomerism. All metallofullerenes exhibited single-molecule magnetism with an open magnetic hysteresis but with a considerably different blocking temperature of magnetization. Dy₂C₂@C₈₈ isomers are weak SMMs with hysteresis closing already at 2.5 K, whereas in Dy₂O@C₈₈ isomers the hysteresis remained open up to 7–9 K. This difference in relaxation behavior agrees with the much stronger single-ion magnetic anisotropy in Dy₂O@C₈₈ than in Dy₂C₂@C₈₈ predicted by *ab initio* calculations.

Conflicts of interest

There are no conflicts to declare.

Acknowledgements

The authors acknowledge financial support by Deutsche Forschungsgemeinschaft (grants PO 1602/7-1, LI 3055/3-1, and AV 169/3-1) and the National Science Foundation China (NSFC 91961109 to N. C.). Diffraction data have been collected on BL14.2 at the BESSY II electron storage ring operated by the Helmholtz-Zentrum Berlin; we would particularly like to acknowledge the help and support of Manfred Weiss and his group members during the experiments at BESSY II. Computational resources were provided by the Center for High Performance Computing at the TU Dresden. We appreciate the technical support with computational resources in IFW Dresden by Ulrike Nitzsche. Sandra Schiemenz is acknowledged for the help with spectroscopic measurements, and Dr Anja Wolter-Giraud and Sebastian Gaß are acknowledged for the help with magnetic measurements in IFW Dresden.

References

- 1 A. A. Popov, S. Yang and L. Dunsch, Endohedral Fullerenes, *Chem. Rev.*, 2013, **113**(8), 5989–6113.
- 2 A. Rodriguez-Forteza, A. L. Balch and J. M. Poblet, Endohedral metallofullerenes: a unique host-guest association, *Chem. Soc. Rev.*, 2011, **40**, 3551–3563.
- 3 X. Lu, W. Shen and S. Hu, Endohedral Metallofullerenes: New Structures and Unseen Phenomena, *Chem. – Eur. J.*, 2020, **26**(26), 5748–5757.
- 4 W. Li, C.-R. Wang and T. Wang, Molecular Structures and Magnetic Properties of Endohedral Metallofullerenes, *Chem. Commun.*, 2021, **57**, 10317–10326.



- 5 W. Cai, C.-H. Chen, N. Chen and L. Echegoyen, Fullerenes as Nanocontainers That Stabilize Unique Actinide Species Inside: Structures, Formation, and Reactivity, *Acc. Chem. Res.*, 2019, **52**(7), 1824–1833.
- 6 S. Yang, T. Wei and F. Jin, When metal clusters meet carbon cages: endohedral clusterfullerenes, *Chem. Soc. Rev.*, 2017, **46**(16), 5005–5058.
- 7 S. Yang, F. Liu, C. Chen, M. Jiao and T. Wei, Fullerenes encaging metal clusters-clusterfullerenes, *Chem. Commun.*, 2011, **47**(43), 11822–11839.
- 8 L. Abella, Y. Wang, A. Rodríguez-Fortea, N. Chen and J. M. Poblet, Current status of oxide clusterfullerenes, *Inorg. Chim. Acta*, 2017, **468**, 91–104.
- 9 L. Feng, Y. Hao, A. Liu and Z. Slanina, Trapping Metallic Oxide Clusters inside Fullerene Cages, *Acc. Chem. Res.*, 2019, **52**(7), 1802–1811.
- 10 X. Lu, T. Akasaka and S. Nagase, Carbide Cluster Metallofullerenes: Structure, Properties, and Possible Origin, *Acc. Chem. Res.*, 2013, **46**(7), 1627–1635.
- 11 P. Jin, C. Tang and Z. Chen, Carbon Atoms Trapped in Cages: Metal Carbide Clusterfullerenes, *Coord. Chem. Rev.*, 2014, **270–271**, 89–111.
- 12 B. Q. Mercado, M. M. Olmstead, C. M. Beavers, M. L. Easterling, S. Stevenson, M. A. Mackey, C. E. Coumbe, J. D. Phillips, J. P. Phillips, J. M. Poblet and A. L. Balch, A seven atom cluster in a carbon cage, the crystallographically determined structure of $\text{Sc}_4(\mu_3\text{-O})_3@I_h\text{-C}_{80}$, *Chem. Commun.*, 2010, **46**, 279–281.
- 13 S. Stevenson, M. A. Mackey, M. A. Stuart, J. P. Phillips, M. L. Easterling, C. J. Chancellor, M. M. Olmstead and A. L. Balch, A Distorted Tetrahedral Metal Oxide Cluster inside an Icosahedral Carbon Cage. Synthesis, Isolation, and Structural Characterization of $\text{Sc}_4(\mu_3\text{-O})_2@I_h\text{-C}_{80}$, *J. Am. Chem. Soc.*, 2008, **130**(36), 11844–11845.
- 14 B. Q. Mercado, M. A. Stuart, M. A. Mackey, J. E. Pickens, B. S. Confait, S. Stevenson, M. L. Easterling, R. Valencia, A. Rodríguez-Fortea, J. M. Poblet, M. M. Olmstead and A. L. Balch, $\text{Sc}_2(\mu_2\text{-O})$ Trapped in a Fullerene Cage: The Isolation and Structural Characterization of $\text{Sc}_2(\mu_2\text{-O})@C_{82}$ and the Relevance of the Thermal and Entropic Effects in Fullerene Isomer Selection, *J. Am. Chem. Soc.*, 2010, **132**, 12098–12105.
- 15 Q. Tang, L. Abella, Y. Hao, X. Li, Y. Wan, A. Rodríguez-Fortea, J. M. Poblet, L. Feng and N. Chen, $\text{Sc}_2\text{O}@C_{3v}(8)\text{-C}_{82}$: A Missing Isomer of $\text{Sc}_2\text{O}@C_{82}$, *Inorg. Chem.*, 2016, **55**(4), 1926–1933.
- 16 L. Feng, M. Zhang, Y. Hao, Q. Tang, N. Chen, Z. Slanina and F. Uhlik, Endohedrally Stabilized C_{70} Isomer with Fused Pentagons Characterized by Crystallography, *Dalton Trans.*, 2016, **45**, 8142–8148.
- 17 Y. Hao, Q. Tang, X. Li, M. Zhang, Y. Wan, L. Feng, N. Chen, Z. Slanina, L. Adamowicz and F. Uhlik, Isomeric $\text{Sc}_2\text{O}@C_{78}$ Related by a Single-Step Stone–Wales Transformation: Key Links in an Unprecedented Fullerene Formation Pathway, *Inorg. Chem.*, 2016, **55**(21), 11354–11361.
- 18 T. Yang, Y. Hao, L. Abella, Q. Tang, X. Li, Y. Wan, A. Rodríguez-Fortea, J. M. Poblet, L. Feng and N. Chen, $\text{Sc}_2\text{O}@T_d(19151)\text{-C}_{76}$: Hindered Cluster Motion inside a Tetrahedral Carbon Cage Probed by Crystallographic and Computational Studies, *Chem. – Eur. J.*, 2015, **21**(31), 11110–11117.
- 19 Q. Tang, L. Abella, Y. Hao, X. Li, Y. Wan, A. Rodríguez-Fortea, J. M. Poblet, L. Feng and N. Chen, $\text{Sc}_2\text{O}@C_{2v}(5)\text{-C}_{80}$: Dimetallic Oxide Cluster Inside a C_{80} Fullerene Cage, *Inorg. Chem.*, 2015, **54**(20), 9845–9852.
- 20 M. Zhang, Y. Hao, X. Li, L. Feng, T. Yang, Y. Wan, N. Chen, Z. Slanina, F. Uhlik and H. Cong, Facile Synthesis of an Extensive Family of $\text{Sc}_2\text{O}@C_{2n}$ ($n = 35\text{--}47$) and Chemical Insight into the Smallest Member of $\text{Sc}_2\text{O}@C_2(7892)\text{-C}_{70}$, *J. Phys. Chem. C*, 2014, **118**(49), 28883–28889.
- 21 A. Liu, M. Nie, Y. Hao, Y. Yang, T. Wang, Z. Slanina, H. Cong, L. Feng, C. Wang and F. Uhlik, $\text{Ho}_2\text{O}@C_{74}$: Ho_2O Cluster Expands within a Small Non-IPR Fullerene Cage of $C_2(13333)\text{-C}_{74}$, *Inorg. Chem.*, 2019, **58**(8), 4774–4781.
- 22 H. Cong, A. Liu, Y. Hao, L. Feng, Z. Slanina and F. Uhlik, $\text{Ho}_2\text{O}@C_{84}$: Crystallographic Evidence Showing Linear Metallic Oxide Cluster Encapsulated in IPR Fullerene Cage of $D_{2d}(51591)\text{-C}_{84}$, *Inorg. Chem.*, 2019, **58**(16), 10905–10911.
- 23 W. Dong, Y. Yu, B. Dong and Y. Lian, Isolation and Electrochemical Property of $\text{Ho}_2\text{O}@C_{90}$ Isomers, *J. Electrochem. Soc.*, 2022, **169**(2), 026512.
- 24 Y. Yu, Z. Slanina, F. Wang, Y. Yang, Y. Lian, F. Uhlik, B. Xin and L. Feng, $\text{Ho}_2\text{O}@D_3(85)\text{-C}_{92}$: Highly Stretched Cluster Dictated by a Giant Cage and Unexplored Isomerization, *Inorg. Chem.*, 2020, **59**(15), 11020–11027.
- 25 G. Velkos, W. Yang, Y.-R. Yao, S. M. Sudarkova, X. Liu, B. Büchner, S. M. Avdoshenko, N. Chen and A. A. Popov, Shape-adaptive single-molecule magnetism and hysteresis up to 14 K in oxide clusterfullerenes $\text{Dy}_2\text{O}@C_{72}$ and $\text{Dy}_2\text{O}@C_{74}$ with fused pentagon pairs and flexible $\text{Dy}-(\mu_2\text{-O})\text{-Dy}$ angle, *Chem. Sci.*, 2020, **11**, 4766–4772.
- 26 G. Velkos, W. Yang, Y.-R. Yao, S. M. Sudarkova, F. Liu, S. Avdoshenko, N. Chen and A. A. Popov, Metallofullerene single-molecule magnet $\text{Dy}_2\text{O}@C_{2v}(5)\text{-C}_{80}$ with a strong antiferromagnetic $\text{Dy}\cdots\text{Dy}$ coupling, *Chem. Commun.*, 2022, **58**, 7164–7167.
- 27 W. Yang, G. Velkos, F. Liu, S. M. Sudarkova, Y. Wang, J. Zhuang, H. Zhang, X. Li, X. Zhang, B. Büchner, S. M. Avdoshenko, A. A. Popov and N. Chen, Single Molecule Magnetism with Strong Magnetic Anisotropy and Enhanced $\text{Dy}\cdots\text{Dy}$ Coupling in Three Isomers of Dy-Oxide Clusterfullerene $\text{Dy}_2\text{O}@C_{82}$, *Adv. Sci.*, 2019, **6**(20), 1901352.
- 28 L. Bao, P. Yu, M.-Y. Li, W. Shen, S. Hu, P. Yu, X. Tian, X. Zhao and X. Lu, An unprecedented C_{80} cage that violates the isolated pentagon rule, *Inorg. Chem. Front.*, 2022, **9**, 2264–2270.
- 29 L. Spree and A. A. Popov, Recent advances in single molecule magnetism of dysprosium-metallofullerenes, *Dalton Trans.*, 2019, **48**(9), 2861–2871.
- 30 H. Yang, H. Jin, B. Hong, Z. Liu, C. M. Beavers, H. Zhen, Z. Wang, B. Q. Mercado, M. M. Olmstead and A. L. Balch,



- Large Endohedral Fullerenes Containing Two Metal Ions, $\text{Sm}_2@D_2(35)\text{-C}_{88}$, $\text{Sm}_2@C_1(21)\text{-C}_{90}$, and $\text{Sm}_2@D_3(85)\text{-C}_{92}$, and Their Relationship to Endohedral Fullerenes Containing Two Gadolinium Ions, *J. Am. Chem. Soc.*, 2011, **133**(42), 16911–16919.
- 31 W. Shen, L. Bao, S. Hu, L. Yang, P. Jin, Y. Xie, T. Akasaka and X. Lu, Crystallographic characterization of Lu_2C_{2n} ($2n = 76\text{--}90$): cluster selection by cage size, *Chem. Sci.*, 2019, **10**(3), 829–836.
- 32 C.-H. Chen, L. Abella, M. R. Cerón, M. A. Guerrero-Ayala, A. Rodríguez-Forteza, M. M. Olmstead, X. B. Powers, A. L. Balch, J. M. Poblet and L. Echegoyen, Zigzag Sc_2C_2 Carbide Cluster inside a [88]Fullerene Cage with One Heptagon, $\text{Sc}_2\text{C}_2@C_s(\text{hept})\text{-C}_{88}$: A Kinetically Trapped Fullerene Formed by C_2 Insertion?, *J. Am. Chem. Soc.*, 2016, **138**(39), 13030–13037.
- 33 C. Pan, W. Shen, L. Yang, L. Bao, Z. Wei, P. Jin, H. Fang, Y.-P. Xie, T. Akasaka and X. Lu, Crystallographic Characterization of Y_2C_{2n} ($2n = 82, 88\text{--}94$): Direct Y-Y Bonding and Cage-Dependent Cluster Evolution, *Chem. Sci.*, 2019, **10**, 4707–4713.
- 34 S. Hu, P. Zhao, W. Shen, M. Ehara, Y. Xie, T. Akasaka and X. Lu, Crystallographic Characterization of $\text{Er}_2\text{C}_2@C_{80\text{--}88}$: Cluster Stretching with Cage Elongation, *Inorg. Chem.*, 2020, **59**(3), 1940–1946.
- 35 W. Shen, L. Bao, P. Yu, L. Yang, B. Li, P. Yu, P. Jin and X. Lu, Isolation and crystallographic characterization of $\text{Lu}_2\text{C}_2@C_{2n}$ ($2n = 88\text{--}92$): Internal cluster stretching upon outer cage expansion, *Carbon*, 2020, **164**, 157–163.
- 36 K. Akiyama, T. Hamano, Y. Nakanishi, E. Takeuchi, S. Noda, Z. Wang, S. Kubuki and H. Shinohara, Non-HPLC Rapid Separation of Metallofullerenes and Empty Cages with TiCl_4 Lewis Acid, *J. Am. Chem. Soc.*, 2012, **134**(23), 9762–9767.
- 37 Z. Wang, Y. Nakanishi, S. Noda, K. Akiyama and H. Shinohara, The Origin and Mechanism of Non-HPLC Purification of Metallofullerenes with TiCl_4 , *J. Phys. Chem. C*, 2012, **116**(48), 25563–25567.
- 38 S. Stevenson, C. B. Rose, A. A. Robson, D. T. Heaps and J. P. Buchanan, Effect of Water and Solvent Selection on the SAFA Purification Times for Metallic Nitride Fullerenes, *Fullerenes, Nanotubes, Carbon Nanostruct.*, 2014, **22**(1–3), 182–189.
- 39 S. Stevenson, K. A. Rottinger and J. S. Field, Fractionation of rare-earth metallofullerenes via reversible uptake and release from reactive silica, *Dalton Trans.*, 2014, **43**(20), 7435–7441.
- 40 S. Stevenson, K. Harich, H. Yu, R. R. Stephen, D. Heaps, C. Coumbe and J. P. Phillips, Nonchromatographic “stir and filter approach” (SAFA) for isolating $\text{Sc}_3\text{N}@C_{80}$ metallofullerenes, *J. Am. Chem. Soc.*, 2006, **128**(27), 8829–8835.
- 41 U. Mueller, R. Förster, M. Hellmig, F. U. Huschmann, A. Kastner, P. Malecki, S. Pühringer, M. Röwer, K. Sparta, M. Steffien, M. Uhllein, P. Wilk and M. S. Weiss, The macromolecular crystallography beamlines at BESSY II of the Helmholtz-Zentrum Berlin: Current status and perspectives, *Eur. Phys. J. Plus*, 2015, **130**(7), 141.
- 42 W. Kabsch, XDS, *Acta Crystallogr., Sect. D: Biol. Crystallogr.*, 2010, **66**(2), 125–132.
- 43 K. M. Sparta, M. Krug, U. Heinemann, U. Mueller and M. S. Weiss, XDSAPP2.0, *J. Appl. Crystallogr.*, 2016, **49**(3), 1085–1092.
- 44 G. Sheldrick, Crystal structure refinement with SHELXL, *Acta Crystallogr., Sect. C: Struct. Chem.*, 2015, **71**(1), 3–8.
- 45 D. S. Krylov, F. Liu, A. Brandenburg, L. Spree, V. Bon, S. Kaskel, A. U. B. Wolter, B. Büchner, S. M. Avdoshenko and A. A. Popov, Magnetization relaxation in the single-ion magnet $\text{DySc}_2\text{N}@C_{80}$: quantum tunneling, magnetic dilution, and unconventional temperature dependence, *Phys. Chem. Chem. Phys.*, 2018, **20**(17), 11656–11672.
- 46 M. M. Olmstead, T. Zuo, H. C. Dorn, T. Li and A. L. Balch, Metal ion size and the pyramidalization of trimetallic nitride units inside a fullerene cage: Comparisons of the crystal structures of $\text{M}_3\text{N}@I_h\text{-C}_{80}$ ($\text{M} = \text{Gd, Tb, Dy, Ho, Er, Tm, Lu, and Sc}$) and some mixed metal counterparts, *Inorg. Chim. Acta*, 2017, **468**, 321–326.
- 47 M. M. Olmstead, D. A. Costa, K. Maitra, B. C. Noll, S. L. Phillips, P. M. Van Calcar and A. L. Balch, Interaction of curved and flat molecular surfaces. The structures of crystalline compounds composed of fullerene (C_{60} , C_{60}O , C_{70} , and C_{120}O) and metal octaethylporphyrin units, *J. Am. Chem. Soc.*, 1999, **121**(30), 7090–7097.
- 48 V. Dubrovina, L.-H. Gan, B. Büchner, A. A. Popov and S. M. Avdoshenko, Endohedral metal-nitride cluster ordering in metallofullerene– Ni^{III} (OEP) complexes and crystals: a theoretical study, *Phys. Chem. Chem. Phys.*, 2019, **21**, 8197–8200.
- 49 W. Cai, L. Bao, S. Zhao, Y. Xie, T. Akasaka and X. Lu, Anomalous Compression of $D_5(450)\text{-C}_{100}$ by Encapsulating La_2C_2 Cluster instead of La_2 , *J. Am. Chem. Soc.*, 2015, **137**(32), 10292–10296.
- 50 S. F. Yang, A. A. Popov and L. Dunsch, Violating the Isolated Pentagon Rule (IPR): The endohedral Non-IPR cage of $\text{Sc}_3\text{N}@C_{70}$, *Angew. Chem., Int. Ed.*, 2007, **46**(8), 1256–1259.
- 51 A. A. Popov, M. Krause, S. F. Yang, J. Wong and L. Dunsch, C_{78} cage isomerism defined by trimetallic nitride cluster size: A computational and vibrational spectroscopic study, *J. Phys. Chem. B*, 2007, **111**(13), 3363–3369.
- 52 S. Yang, A. A. Popov and L. Dunsch, The role of an asymmetric nitride cluster on a fullerene cage: The Non-IPR endohedral $\text{DySc}_2\text{N}@C_{76}$, *J. Phys. Chem. B*, 2007, **111**(49), 13659–13663.
- 53 A. A. Popov, C. Kästner, M. Krause and L. Dunsch, Carbon Cage Vibrations of $\text{M}@C_{82}$ and $\text{M}_2@C_{2n}$ ($\text{M} = \text{La, Ce}$; $2n = 72, 78, 80$): The Role of the Metal Atoms, *Fullerenes, Nanotubes, Carbon Nanostruct.*, 2014, **22**(1–3), 202–214.
- 54 V. Vieru, L. Ungur and L. F. Chibotaru, Key Role of Frustration in Suppression of Magnetization Blocking in Single-Molecule Magnets, *J. Phys. Chem. Lett.*, 2013, **4**(21), 3565–3569.



- 55 M. K. Singh and G. Rajaraman, Acquiring a record barrier height for magnetization reversal in lanthanide encapsulated fullerene molecules using DFT and ab initio calculations, *Chem. Commun.*, 2016, **52**(97), 14047–14050.
- 56 D. S. Krylov, F. Liu, S. M. Avdoshenko, L. Spree, B. Weise, A. Waske, A. U. B. Wolter, B. Büchner and A. A. Popov, Record-high thermal barrier of the relaxation of magnetization in the nitride clusterfullerene Dy₂ScN@C₈₀-I_h, *Chem. Commun.*, 2017, **53**, 7901–7904.
- 57 C.-H. Chen, D. S. Krylov, S. M. Avdoshenko, F. Liu, L. Spree, R. Yadav, A. Alvertis, L. Hozoi, K. Nenkov, A. Kostanyan, T. Greber, A. U. B. Wolter and A. A. Popov, Selective arc-discharge synthesis of Dy₂S-clusterfullerenes and their isomer-dependent single molecule magnetism, *Chem. Sci.*, 2017, **8**(9), 6451–6465.
- 58 A. Brandenburg, D. S. Krylov, A. Beger, A. U. B. Wolter, B. Büchner and A. A. Popov, Carbide clusterfullerene DyYTiC@C₈₀ featuring three different metals in the endohedral cluster and its single-ion magnetism, *Chem. Commun.*, 2018, **54**(76), 10683–10686.
- 59 R. Westerström, V. Dubrovin, K. Junghans, C. Schlesier, B. Büchner, S. M. Avdoshenko, A. A. Popov, A. Kostanyan, J. Dreiser and T. Greber, Precise measurement of angles between two magnetic moments and their configurational stability in single-molecule magnets, *Phys. Rev. B*, 2021, **104**(22), 224401.
- 60 L. Spree, C. Schlesier, A. Kostanyan, R. Westerström, T. Greber, B. Büchner, S. Avdoshenko and A. A. Popov, Single molecule magnets DyM₂N@C₈₀ and Dy₂MN@C₈₀ (M = Sc, Lu): The impact of diamagnetic metals on the Dy³⁺ magnetic anisotropy, Dy...Dy coupling, and mixing of molecular and lattice vibrations, *Chem. – Eur. J.*, 2020, **26**(11), 2436–2449.
- 61 D. Krylov, G. Velkos, C.-H. Chen, B. Büchner, A. Kostanyan, T. Greber, S. Avdoshenko and A. A. Popov, Magnetic hysteresis and strong ferromagnetic coupling of sulfur-bridged Dy ions in clusterfullerene Dy₂S@C₈₂, *Inorg. Chem. Front.*, 2020, **7**, 3521–3532.
- 62 F. Aquilante, J. Autschbach, A. Baiardi, S. Battaglia, V. A. Borin, L. F. Chibotaru, I. Conti, L. D. Vico, M. Delcey, I. F. Galván, N. Ferré, L. Freitag, M. Garavelli, X. Gong, S. Knecht, E. D. Larsson, R. Lindh, M. Lundberg, P. Å. Malmqvist, A. Nenov, J. Norell, M. Odelius, M. Olivucci, T. B. Pedersen, L. Pedraza-González, Q. M. Phung, K. Pierloot, M. Reiher, I. Schapiro, J. Segarra-Martí, F. Segatta, L. Seijo, S. Sen, D.-C. Sergentu, C. J. Stein, L. Ungur, M. Vacher, A. Valentini and V. Veryazov, Modern quantum chemistry with [Open]Molcas, *J. Chem. Phys.*, 2020, **152**(21), 214117.
- 63 L. F. Chibotaru and L. Ungur, Ab initio calculation of anisotropic magnetic properties of complexes. I. Unique definition of pseudospin Hamiltonians and their derivation, *J. Chem. Phys.*, 2012, **137**(6), 064112.
- 64 X. Yi, K. Bernot, F. Pointillart, G. Poneti, G. Calvez, C. Daguebonne, O. Guillou and R. Sessoli, A Luminescent and Sublimable Dy^{III}-Based Single-Molecule Magnet, *Chem. – Eur. J.*, 2012, **18**(36), 11379–11387.
- 65 J. Long, F. Habib, P.-H. Lin, I. Korobkov, G. Enright, L. Ungur, W. Wernsdorfer, L. F. Chibotaru and M. Murugesu, Single-Molecule Magnet Behavior for an Antiferromagnetically Superexchange-Coupled Dinuclear Dysprosium(III) Complex, *J. Am. Chem. Soc.*, 2011, **133**(14), 5319–5328.
- 66 S. A. Sulway, R. A. Layfield, F. Tuna, W. Wernsdorfer and R. E. P. Winpenny, Single-molecule magnetism in cyclopentadienyl-dysprosium chlorides, *Chem. Commun.*, 2012, **48**(10), 1508–1510.
- 67 S. Xue, Y.-N. Guo, L. Ungur, J. Tang and L. F. Chibotaru, Tuning the Magnetic Interactions and Relaxation Dynamics of Dy₂ Single-Molecule Magnets, *Chem. – Eur. J.*, 2015, **21**(40), 14099–14106.
- 68 C. Y. Chow, H. Bolvin, V. E. Campbell, R. Guillot, J. W. Kampf, W. Wernsdorfer, F. Gendron, J. Autschbach, V. L. Pecoraro and T. Mallah, Assessing the exchange coupling in binuclear lanthanide(III) complexes and the slow relaxation of the magnetization in the antiferromagnetically coupled Dy₂ derivative, *Chem. Sci.*, 2015, **6**(7), 4148–4159.
- 69 J. Xiong, H.-Y. Ding, Y.-S. Meng, C. Gao, X.-J. Zhang, Z.-S. Meng, Y.-Q. Zhang, W. Shi, B.-W. Wang and S. Gao, Hydroxide-bridged five-coordinate Dy^{III} single-molecule magnet exhibiting the record thermal relaxation barrier of magnetization among lanthanide-only dimers, *Chem. Sci.*, 2017, **8**(2), 1288–1294.
- 70 G. Huang, X. Yi, J. Jung, O. Guillou, O. Cador, F. Pointillart, B. Le Guennic and K. Bernot, Optimization of Magnetic Relaxation and Isotopic Enrichment in Dimeric Dy^{III} Single-Molecule Magnets, *Eur. J. Inorg. Chem.*, 2018, **2018**, 326–332.
- 71 P.-B. Jin, Q.-C. Luo, Y.-Q. Zhai, Y.-D. Wang, Y. Ma, L. Tian, X. Zhang, C. Ke, X.-F. Zhang, Y. Lv and Y.-Z. Zheng, A study of cation-dependent inverse hydrogen bonds and magnetic exchange-couplings in lanthanacarborane complexes, *iScience*, 2021, **24**(7), 102760.
- 72 N. F. Chilton, R. P. Anderson, L. D. Turner, A. Soncini and K. S. Murray, PHI: A powerful new program for the analysis of anisotropic monomeric and exchange-coupled polynuclear d- and f-block complexes, *J. Comput. Chem.*, 2013, **34**(13), 1164–1175.
- 73 R. Westerström, J. Dreiser, C. Piamonteze, M. Muntwiler, S. Weyeneth, K. Krämer, S.-X. Liu, S. Decurtins, A. Popov, S. Yang, L. Dunsch and T. Greber, Tunneling, remanence, and frustration in dysprosium-based endohedral single-molecule magnets, *Phys. Rev. B: Condens. Matter Mater. Phys.*, 2014, **89**(6), 060406.
- 74 A. Kostanyan, R. Westerström, D. Kunhardt, B. Büchner, A. A. Popov and T. Greber, Sub-Kelvin hysteresis of the dilanthanide single-molecule magnet Tb₂ScN@C₈₀, *Phys. Rev. B*, 2020, **101**(13), 134429.
- 75 Y.-N. Guo, G.-F. Xu, W. Wernsdorfer, L. Ungur, Y. Guo, J. Tang, H.-J. Zhang, L. F. Chibotaru and A. K. Powell,



- Strong Axiality and Ising Exchange Interaction Suppress Zero-Field Tunneling of Magnetization of an Asymmetric Dy₂ Single-Molecule Magnet, *J. Am. Chem. Soc.*, 2011, **133**(31), 11948–11951.
- 76 T. G. Ashebr, H. Li, X. Ying, X.-L. Li, C. Zhao, S. Liu and J. Tang, Emerging Trends on Designing High-Performance Dysprosium(III) Single-Molecule Magnets, *ACS Mater. Lett.*, 2022, **4**, 307–319.
- 77 A. Zabala-Lekuona, J. M. Seco and E. Colacio, Single-Molecule Magnets: From Mn₁₂-ac to dysprosium metallo-cenes, a travel in time, *Coord. Chem. Rev.*, 2021, **441**, 213984.
- 78 D. Shao and X.-Y. Wang, Development of Single-Molecule Magnets, *Chin. J. Chem.*, 2020, **38**, 1005–1018.
- 79 J.-L. Liu, Y.-C. Chen and M.-L. Tong, Symmetry strategies for high performance lanthanide-based single-molecule magnets, *Chem. Soc. Rev.*, 2018, **47**, 2431–2453.
- 80 K. L. M. Harriman, D. Errulat and M. Murugesu, Magnetic Axiality: Design Principles from Molecules to Materials, *Trends Chem.*, 2019, **1**(4), 425–439.
- 81 A. Singh and K. N. Shrivastava, Optical-acoustic two-phonon relaxation in spin systems, *Phys. Status Solidi B*, 1979, **95**(1), 273–277.
- 82 K. Junghans, C. Schlesier, A. Kostanyan, N. A. Samoylova, Q. Deng, M. Rosenkranz, S. Schiemenz, R. Westerström, T. Greber, B. Büchner and A. A. Popov, Methane as a Selectivity Booster in the Arc-Discharge Synthesis of Endohedral Fullerenes: Selective Synthesis of the Single-Molecule Magnet Dy₂TiC@C₈₀ and Its Congener Dy₂TiC₂@C₈₀, *Angew. Chem., Int. Ed.*, 2015, **54**(45), 13411–13415.
- 83 F. Cimpoesu, N. Dragoe, H. Ramanantoanina, W. Urland and C. Daul, The Theoretical Account of the Ligand Field Bonding Regime and Magnetic Anisotropy in the DySc₂N@C₈₀ Single Ion Magnet Endohedral Fullerene, *Phys. Chem. Chem. Phys.*, 2014, **16**, 11337–11348.
- 84 R. Westerström, J. Dreiser, C. Piamonteze, M. Muntwiler, S. Weyeneth, H. Brune, S. Rusponi, F. Nolting, A. Popov, S. Yang, L. Dunsch and T. Greber, An Endohedral Single-Molecule Magnet with Long Relaxation Times: DySc₂N@C₈₀, *J. Am. Chem. Soc.*, 2012, **134**(24), 9840–9843.
- 85 M. Nie, J. Liang, C. Zhao, Y. Lu, J. Zhang, W. Li, C. Wang and T. Wang, Single-Molecule Magnet with Thermally Activated Delayed Fluorescence Based on a Metallofullerene Integrated by Dysprosium and Yttrium Ions, *ACS Nano*, 2021, **15**(12), 19080–19088.
- 86 W. Cai, J. D. Bocarsly, A. Gomez, R. J. Letona Lee, A. Metta-Magaña, R. Seshadri and L. Echegoyen, High blocking temperatures for DyScS endohedral fullerene single-molecule magnets, *Chem. Sci.*, 2020, **11**, 13129–13136.

